Nanocrystal Formation and Faceting Instability in Al(110) Homoepitaxy: *True* Upward Adatom Diffusion at Step Edges and Island Corners

Francesco Buatier de Mongeot,[1] Wenguang Zhu,[2,3] A. Molle,[1] R. Buzio,[1] C. Boragno,[1] U. Valbusa,[1] E. G. Wang,[2] and Zhenyu Zhang[3,4]

[1]*INFM-Unità di Genova and Dipartimento di Fisica, Università di Genova, Via Dodecaneso 33, I-16146 Genova, Italy*
[2]*ICQS and Institute of Physics, Chinese Academy of Sciences, Beijing 100080, People's Republic of China*
[3]*Condensed Matter Sciences Division, Oak Ridge National Laboratory, Oak Ridge, Tennessee 37831-6032, USA*
[4]*Department of Physics and Astronomy, University of Tennessee, Knoxville, Tennessee 37966, USA*

(Received 19 December 2002; published 2 July 2003)

Using atomic force microscopy and spot-profile analyzing low energy electron diffraction, we have observed the existence of a striking faceting instability in Al(110) homoepitaxy, characterized by the formation of nanocrystals with well-defined facets. These hut-shaped nanocrystals are over tenfold higher than the total film coverage, and coexist in a bimodal growth mode with much shallower and more populous surface mounds. We further use density functional theory calculations to elucidate the microscopic origin of the faceting instability, induced by surprisingly low activation barriers for adatom ascent at step edges and island corners.

DOI: 10.1103/PhysRevLett.91.016102 PACS numbers: 68.55.Jk, 61.14.Hg, 68.35.Ct, 68.37.Ps

Uncovering nature's hidden regulations in building various fascinating crystal shapes has been a primary motivation of research in science. In this endeavor, a crucial concept identified in thin film growth is the so-called step-edge or Ehrlich-Schwoebel (ES) barrier effect, which is kinetic in nature [1–3]. An adatom diffusing on an upper atomic layer will likely encounter an additional potential energy barrier, called the ES barrier, when descending to a lower layer at the edge of its residing terrace [1,2]. Extensive research activities have firmly established two important notions in thin film growth and nanocrystal formation: Smooth films can be achieved only if the ES barrier effect is sufficiently weak, whereas the formation of surface mounds, nanoclusters, and quantum dots may result from strong ES barrier effects [3,4]. In heteroepitaxy, the strain energy associated with the lattice mismatch between the growing material and the substrate is another crucial factor influencing the growth mode. This factor, thermodynamic in nature, competes with the various kinetic factors, thereby significantly enhancing the richness for growth manipulation and control. Interesting extensions of the ES barrier concept have also been made recently to both lower and higher dimensions, corresponding to atom crossing at island corners [4] and at the outer ridge between two facets [5].

In this Letter, we report on striking atomic force microscopy (AFM) and spot-profile analyzing low-energy electron diffraction (SPA-LEED) observations of nanocrystal formation in Al(110) homoepitaxy, an intriguing phenomenon defying interpretation based on prevailing knowledge of growth sketched above. These metastable, hut-shaped nanocrystals are tenfold higher than the average film thickness, can be formed only within a temperature window and only when the total film coverage exceeds a critical value, and coexist with much shallower and more populous surface mounds. Whereas the formation of the mounds can be attributed to insufficient downward adatom diffusion within the framework of an ES barrier effect, the formation of the huts demands massive atom transport from the terrace onto growing huts. Such true upward diffusion events can occur because the activation barriers for adatom ascent at both the step edges and island inner corners are low, as shown by density functional theory (DFT) calculations. The faceting instability observed here and the kinetic picture developed for its interpretation should be applicable to other related growth systems as well.

The growth experiments were performed in a UHV apparatus at a rate of 1 monolayer (ML) per minute. The background pressure during deposition was below 1×10^{-10} mbar. The chemical cleanliness of the surface prior to and after deposition was checked by means of Auger spectroscopy, with an upper limit of oxygen detection below 0.01 ML. After deposition, the substrate temperature was quenched to 80 K within minutes in order to prevent postannealing restructuring of the films. Thereafter the surface morphology was analyzed by SPA-LEED, providing detailed average information on the step distribution and on the presence of facets [6]. The AFM measurements were performed *ex situ* after annealing the sample to room temperature.

Figure 1(a) is an AFM topograph recorded after deposition of 30 ML of aluminum at $T = 450$ K on an atomically flat Al(110) substrate. Here, large clusters elongated along the $\langle 1\bar{1}0 \rangle$ crystallographic direction have been formed on top of a background of much smaller islands. At a closer inspection shown in Fig. 1(c), the large clusters appear to be regular pyramidal huts, bound by four extended facets. A line-profile analysis of the huts along

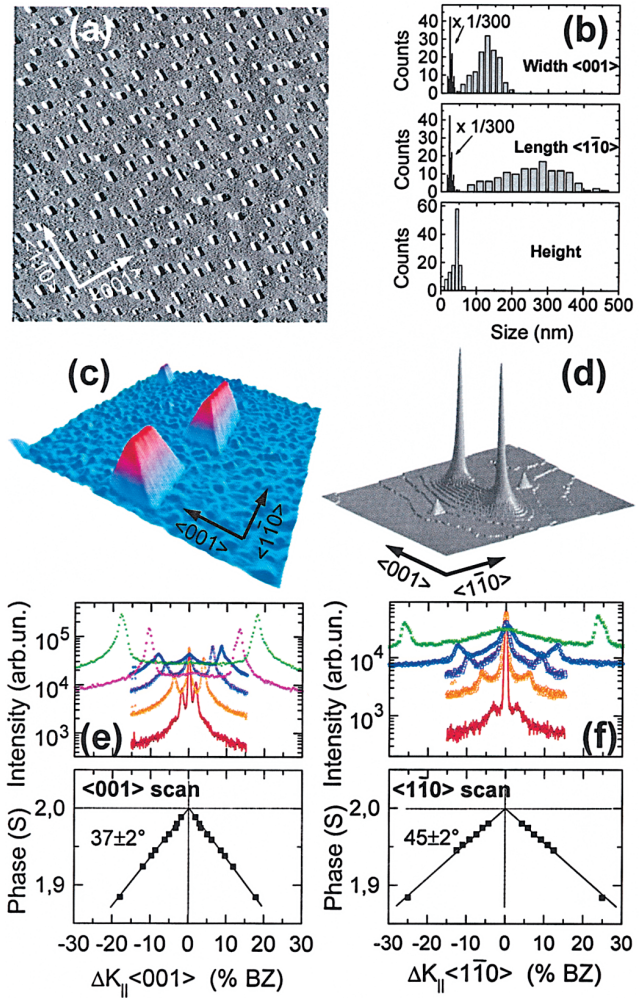

FIG. 1 (color). (a) AFM topograph of the Al(110) surface after deposition of 30 ML of Al at $T = 450$ K (10×10 μm^2). (b) The panels from top to bottom show the histograms of the island width, length, and height distributions. (c) Perspective AFM view at higher magnification, evidencing the nanocluster facets (1×1 μm^2). (d) The 2D diffraction pattern of the (00) spot recorded by SPA-LEED near out-of-phase conditions ($E = 68.6$ eV, vertical scattering phase $S = 1.91$, scan size 97% of the Brillouin zone) after deposition of 30 ML of Al at $T = 450$ K. (e) The 1D SPA-LEED scans of the (00) diffraction spot across the major satellites. The slope of the satellite splitting vs the scattering phase S measures the contact angle of the facets with respect to the (110) terrace. (f) Same as in (e) but across the minor satellites.

the two principal crystallographic directions of $\langle 001 \rangle$ and $\langle 1\bar{1}0 \rangle$ reveals that the facets form angles of $36° \pm 2°$ and $45° \pm 2°$ with respect to the base plane, respectively. In the magnified view shown in Fig. 1(c) it is also more evident that the background consists of much smaller and more populous three-dimensional (3D) islands (mounds), with an average height of the order of 2 nm. The distributions of the dimensions of the hut nanocrystals are plotted in Fig. 1(b). The upper panel shows the distribution of the widths (grey bars), which are peaked around 130 nm; also plotted (black bars) is the distribution of the diameters of the shallow mounds in the background, scaled down by a factor of 300. In the middle panel the histogram of the lengths of the huts is plotted, showing a uniform distribution in the range of (100–400) nm. Finally, the lower panel shows the distribution of the heights of the huts, peaked around 50 nm (due to resolution limitations of the AFM, the statistics of the mounds in the background are omitted). Collectively, the AFM patterns demonstrate qualitatively and quantitatively the existence of a bimodal growth mode, signified by a family of hut-shaped nanocrystals in competition with a zoo of shallow mounds in the background. As an independent confirmation of the nanocrystal morphology, the facet orientations were also determined *in situ* during growth by SPA-LEED. Figure 1(d) shows a 2D map of the (00) diffraction spot from the film shown in Fig. 1(a). The spot appears split along the high symmetry directions into two pairs of satellites, induced, respectively, by diffraction from the major and minor facets of the huts. A measurement of the satellite splitting vs electron energy, corresponding to varying the vertical scattering phase S in Figs. 1(e) and 1(f), yields the slopes of the facets (bottom panels), which are very close to the slopes observed *ex situ* by AFM. We therefore can conclude that the {111} and {100} planes terminate the major and minor facets of the huts, respectively.

In order to identify the kinetic conditions under which nanocrystal formation takes place, a thorough *in situ* SPA-LEED analysis of the growth process has been performed as a function of the substrate temperature and film coverage. The results are summarized as follows. (a) There is a temperature window between 330 K and ~500 K within which the formation of the huts is competitive with mound formation. Figure 2(a) shows a sequence of 1D scans of the (00) diffraction peak recorded along $\langle 001 \rangle$ at different substrate temperatures, but with the same coverage of 30 ML. For temperatures of 250 and 280 K, the diffraction peaks are broad and unstructured, corresponding to a facet-free background. Only above 330 K do two satellites become observable, but the broad FWHM of the satellites indicates that the width of (111) facets is still small. A dramatic tenfold decrease of the satellite width is observed when the deposition temperature increases from 330 to 380 K due to the enlargement of the (111) facets, which are highly favored in the growth of the nanocrystals. (b) At a given temperature of 380 K or higher, hut formation still requires a critical film coverage of about 10 ML. In Fig. 2(b) a sequence of 1D scans of the (00) spot is plotted as a function of the Al coverage. At 2 and 4 ML, no well defined slope selection is observed. Only at a critical coverage of ~10 ML do satellites appear. In the whole coverage range above 10 ML, a well-defined slope selection is found, corresponding to the formation of the (111) facets. (c) The huts are metastable: If the deposition flux is stopped, they begin to decay above 450 K while approximately maintaining the (111) slope [Fig. 2(c)].

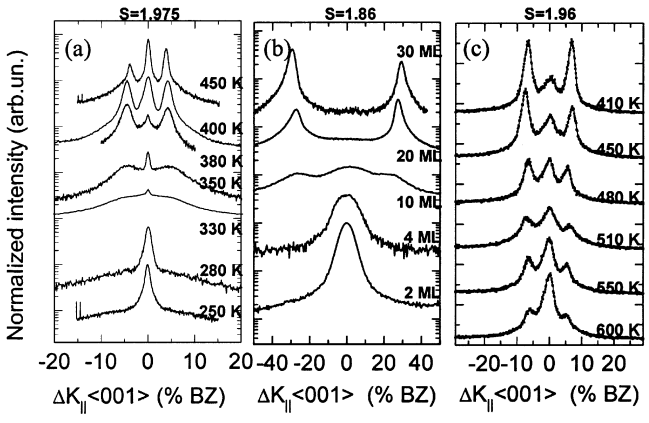

FIG. 2. The 1D SPA-LEED scans of the (00) diffraction spots across the major satellites under different growth conditions. (a) After deposition of 30 ML of Al at different temperatures ($E = 73$ eV, $S = 1.975$). (b) Increasing Al thickness at a fixed deposition temperature of $T = 380$ K ($E = 65$ eV, $S = 1.86$). (c) Thermal stability of the huts upon annealing for 60 sec at the given temperature after deposition of 30 ML of Al at $T = 450$ K ($E = 72$ eV, $S = 1.96$).

Quantitatively, the height of the background mounds is typical for kinetic roughening in metal homoepitaxy [7,8]. In contrast, the peaked height of the huts, at 50 nm, is over tenfold higher than the deposited film thickness of 4.3 nm. This seems to be the first known example showing such a dramatic singular growth phenomenon in a homoepitaxial system. These hut nanocrystals are also much taller than the faceted islands in several widely studied heteroepitaxial growth systems [9–11]. We stress that, unlike the faceted islands in heteroepitaxial systems, the dominant driving force for the formation of the nanocrystals in the present homoepitaxial system cannot be due to stress. Furthermore, their formation cannot be attributed to the primary effects of minute amounts of contaminants in the deposition flux or preadsorbed on the substrate, as it would require much higher coverages of such adsorbates to induce faceting [11]. The metastability of these nanocrystals also strongly indicates that the dominant formation mechanism should be kinetic in nature.

Next we attempt to gain a microscopic understanding of these striking observations. Because of their morphological similarity with existing studies of metal homoepitaxy [7,8], we tentatively attribute the growth of the surface mounds to the kinetic limitations associated with an effective upward diffusion current in the growth front [3]. On the other hand, the exceptionally large heights of the huts must call for an unusual kinetic mechanism involving *true* and massive upward adatom transport from the surface onto the hut nanocrystals. In order to understand why such true upward diffusion could ever be possible, we have used the Vienna *ab initio* simulation package within the generalized gradient approximation (VASP/GGA) [12] to calculate all the essential diffusion processes involved, which are summarized in Fig. 3. The biggest surprises from these DFT calculations are twofold. First, contrary to prevailing belief, the activation barriers for atom ascent at step edges along both the $\langle 001 \rangle$ and $\langle 1\bar{1}0 \rangle$ directions are relatively low, equal to 0.67 and 0.60 eV, respectively. As shown in Figs. 3(a) and 3(b), these ascending processes are easily feasible via the place exchange mechanism. In fact, along the $\langle 001 \rangle$ direction the exchange process for atom ascent is even slightly favored over the reverse exchange process for atom descent, by 0.04 eV, and both barriers are comparable to the cross-channel adatom diffusion barrier of 0.49 eV [see Fig. 3(d)]. Therefore, at growth temperatures where terrace diffusion on the (110) surface can proceed in both the in-channel and cross-channel directions, adatom-ascending events can also be readily activated. The second surprise is illustrated by the *B* to *A* process shown in Figs. 3(c) and 3(d), where the activation barrier for an adatom to leave an inner-corner site and climb upwards onto an (100) or (111) facet is also relatively low, equal to 0.69 and 0.70 eV, respectively. We note that both types of upward diffusion events were typically ignored in earlier studies of thin film growth, because they were perceived to require much higher activation energies.

In developing a more complete view of the faceting instability, several additional observations need to be made based on our present VASP/GGA calculations [13]. (a) Once overcoming the inner-corner crossing barrier, an adatom can diffuse very fast on the (111) or (100) facet, with an activation energy of 0.04 or 0.19 eV, respectively [14]. (b) The so-called 3D-ES barriers for outer-corner crossing [5] are highly asymmetric, favoring the transport of adatoms from the (111) and (100) facets onto the top of a hut island (*D* to *C* process), with activation barriers of 0.04 versus 0.69 eV and 0.13 versus

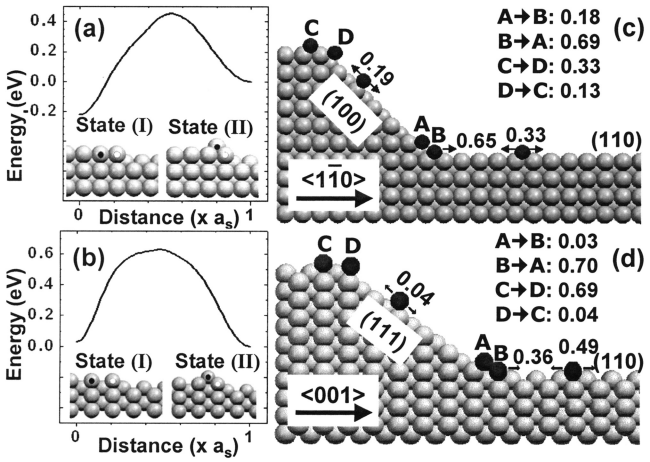

FIG. 3. Activation energies for various kinetic processes discussed in the text. (a),(b) Adatom ascent at the step edge via place exchange along the $\langle 1\bar{1}0 \rangle$ and $\langle 001 \rangle$ directions, respectively. (c),(d) Energy barriers against surface and terrace diffusion, inner-corner crossing and outer-corner crossing along the $\langle 1\bar{1}0 \rangle$ and $\langle 001 \rangle$ directions, respectively.

0.33 eV, respectively. (c) The 3D-ES barriers for outer-corner crossing between the (111) and (100) facets are also asymmetric, favoring the transport of adatoms from the (111) facets to the (100) facets, with activation barriers of 0.08 versus 0.53 eV (not shown in Fig. 3). (d) The detachment of a lone adatom from a step edge is relatively easy, corresponding to an activation barrier of 0.45 and 0.57 eV along the $\langle 001 \rangle$ and $\langle 1\bar{1}0 \rangle$ directions, respectively.

Given the various kinetic processes described above, we can envision the following picture for the faceting instability via bimodal growth in Al(110) homoepitaxy. As the film grows, roughness in the growth front will be developed as a result of the standard ES barrier effect. To account for the dramatic instability leading to the hut islands, *true* and frequent upward adatom diffusion events must be present in the growth front. These upward diffusion events are of two types. The first type is the ascending processes at step edges shown in Figs. 3(a) and 3(b); the second type is the inner-corner crossing processes (B to A) shown in Figs. 3(c) and 3(d). The first type is active whenever steps are present, and qualitatively, it can enhance the roughening instability induced by the standard ES barrier effect. The second type becomes active only after mini-(100) and (111) facets have been created as a result of large-scale fluctuations in the growth morphology. Such well-defined facets are not only energetically more favorable than the mounds with rough edges, but, more importantly, they can provide fast channels for transporting adatoms that have managed to cross the inner corners located at their bases to the upper edges of the facets. There, these adatoms can easily overcome the asymmetric outer-corner-crossing barriers to reach the tops of the islands; also, the asymmetric rate processes for outer-corner crossing between the (111) and the (100) facets efficiently transport adatoms from the (111) facets onto the (100) facets, favoring nucleation and growth along the in-channel direction.

A complete confirmation of the above picture by 3D kinetic Monte Carlo (KMC) simulations is too demanding and beyond the scope of the present study. Nevertheless, our preliminary results of (1 + 1)D KMC simulations along both the in-channel and cross-channel directions confirm the validity of the picture in many essential ways [13]. Before closing, we also stress that the relative easiness for true upward adatom diffusion identified here should not be limited to the present system of Al(110) homoepitaxy alone. At least, we expect such processes to be easily feasible in other metal fcc(110) systems, which show evidence of faceting [15].

In summary, we have discovered a striking faceting instability via bimodal growth in Al(110) homoepitaxy, characterized by the coexistence of unusually tall nanocrystals with well-defined facets and much shallower and more populous surface mounds. The hut-shaped nanocrystals are metastable, and can be formed only within a growth temperature window and when the total coverage exceeds a critical value. Efforts to interpret these intriguing observations at the microscopic level have shown that upward adatom diffusion by ascending at step edges and/or inner-corner crossing, thought to be negligible in most (if not all) previous studies of film growth, can actually be activated rather easily. Inclusion of such true upward diffusion events in connection with the widely studied ES barrier effect and the effect of stress will undoubtedly enrich the nature of instabilities in various metal (110) and other related homoepitaxial/heteroepitaxial growth systems.

Useful discussions with R. Ferrando, M. G. Lagally, J. Tersoff, and J. F. Wendelken are acknowledged. This work has been supported in part by INFM under the project PRA-Nanorub, by ORNL, managed by UT-Battell, LLC, for the U.S. DOE under Contract No. DE-AC05-00OR22725, by U.S. NSF, and by the NSF and MOST of China.

[1] G. Ehrlich and F. G. Hudda, J. Phys. Chem. **44**, 1939 (1966).
[2] R. L. Schwoebel and E. J. Shipsey, J. Appl. Phys. **37**, 3682 (1966).
[3] J. Villain, J. Phys. I (France) **1**, 19 (1991).
[4] Z. Y. Zhang and M. G. Lagally, Science **76**, 377 (1997).
[5] S. J. Liu, H. C. Huang, and C. H. Woo, Appl. Phys. Lett. **80**, 3295 (2002); M. G. Lagally and Z. Y. Zhang, Nature (London) **417**, 907 (2002).
[6] F. Buatier de Mongeot *et al.*, Phys. Rev. Lett. **84**, 2445 (2000).
[7] J. A. Stroscio *et al.*, Phys. Rev. Lett. **75**, 4246 (1995).
[8] L. C. Jorritsma, M. Bijnagte, G. Rosenfeld, and B. Poelsema, Phys. Rev. Lett. **78**, 919 (1997).
[9] G. Medeiro-Ribeiro *et al.*, Science **279**, 353 (1998).
[10] For a review, see V. A. Shchukin and D. Bimberg, Rev. Mod. Phys. **71**, 1125 (1999).
[11] T. E. Madey *et al.*, Surf. Sci. **438**, 191 (1999).
[12] G. Kresse and J. Hafner, Phys. Rev. B **47**, 558 (1993); **49**, 14 251 (1994).
[13] W. G. Zhu *et al.* (to be published).
[14] The activation energies obtained here within the GGA, whenever comparable, are systematically lower than the results obtained in an earlier study within the LDA approximation by R. Stumpf and M. Scheffler, Phys. Rev. B **53**, 4958 (1996).
[15] D. Tian, F. Jona, and P. M. Marcus, Phys. Rev. B **45**, 11 216 (1992); K. Fang, T.-M. Lu, and G.-C.Wang, Phys. Rev. B **49**, 8331 (1994); J. Shen, J. Giergiel, A. K. Schmid, and J. Kirschner, Surf. Sci. **328**, 32 (1995); R. Persaud, H. Noro, and J. A. Venables, Surf. Sci. **401**, 12 (1998); S. Tacchi *et al.*, Surf. Sci. **507**, 324 (2002).